# Regeneration of NCM622 from end-of-life lithium-ion batteries cathode materials

Shuai Gu[a,b,*], Ting He[a,b], Jiao Kong[a,b], Tongtong Fu[c], Zirui Guo[c], Jingzhi Cui[c], Zhihao Chen[c]

[a] National Engineering Research Center for Integrated Utilization of Salt Lake Resources, East China University of Science and Technology, Shanghai, 200237, China

[b] Joint International Laboratory for Potassium and Lithium Strategic Resources, East China University of Science and Technology, Shanghai, 200237, China

[c] School of Chemical Engineering, East China University of Science and Technology, Shanghai 200237, China

*Corresponding contributor. E-mail: gushuai@ecust.edu.cn

## Contents

**Table S1** XRF and EDX analysis of EOL cathode material.

**Table S2** Leaching efficiency results of Li (a), Co (b), Ni (c), and Mn (d) with various acids ratios at 40 min and 10 g/L solid-liquid ratio.

**Table S3** The amount of VC required to treat 2 kg of spent lithium-ion batteries.

**Table S4** Leaching efficiencies and EDX analysis of the leached cathode material.

**Table S5**XPS parameters obtained from the leached spent cathode materials.

**Table S6** Variation of metal concentration in recovery process.

**Table S7** A comprehensive summary of the kinetic models.

**Table S8** Regression parameters of Li, Co, Ni, and Mn.

**Table S9** Lattice structure parameters of the NCM622 cathode material.

**Figure S1** EOL LIBs (a), cathode (b), and recovered cathode powders (c) from EOL LIBs.

**Figure S2** Leaching kinetics of Co at 30 ℃ and 10 g/L solid-liquid ratio at 11min (a), 20 min (b), 30 min (c), and 40min (d) with various mixed acids ratios.

**Figure S3** Correlation and significance between mixed acids ratios and leaching efficiencies (a), Eh-pH diagram measured during the leaching process with 0.5 M HCl, 0.25 M $HNO_3$, and 0.25 M HCl at 30 °C and 10 g/L solid-liquid ratio (b).

**Figure S4** Leaching kinetics of strategic metals at 30 °C (a), 50 °C (b), 70 °C (c), and 90 °C (d) at 10 g/L solid-liquid ratio, 0.5 M HCl, 0.25 M $HNO_3$ and 0.25 M VC.

**Figure S5** SEM (a) and EDX (b) images of the leached residual at 90 ℃ with optimal acids ratios.

**Figure S6** XPS survey of the leached residual at 30 °C (a) and the deconvoluted high-resolution XPS curves of Co (b), O (c), and Al (d).

**Figure S7** Thermodynamic calculations of Ni-containing (a) and Mn-containing (b) species at 30°C.

**Figure S8** Reactions of DHA hydrate to form Bi-DHA.

**Figure S9** Thermodynamic calculated species distributions of mixed acids system at 30 ℃ (a), 50 ℃ (b), 70 ℃ (c) and 90 ℃ (d).

**Figure S10** UV-vis spectrum of mixed acids at 0min (a), 1~40 min (b), and deconvoluted absorbance curves at 1 min (c) and 40 min (d).

**Figure S11** Deconvoluted UV-vis absorbance in mixed acids system at 5 min (a), 7 min (b), 11 min (c), and 20 min (d).

**Figure S12** SEM (c), and EDX (d) images of the as-recovered NCM622 precursor.

**Materials**

All spent LIBs cathode materials utilized in this study were dismantled from spent mobile phone batteries purchased from Alibaba Group Holding Ltd. Hydrochloric acid (HCl, AR, 35 ~ 38%, Sinopharm Chemical Reagent Co., Ltd.), nitric acid ($HNO_3$, AR, 65 ~ 68%) and L-ascorbic acid ($C_6H_8O_6$, AR, purity > 99.0%) were dissolved/diluted before use. Ammonium hydroxide aqueous solution ($NH_3H_2O$, CP, 25 ~ 28%) is used to adjust the pH of the effluent. Sodium carbonate ($Na_2CO_3$, CP, purity ⩾99.8%) for precipitation of NCM622 precursor and $Li_2CO_3$. Lithium carbonate ($Li_2CO_3$, 4N, purity > 99.5%) for precipitation of NCM622 precursor. And the recovered $Li_2CO_3$ can be utilized in the manufacturing of NCM 622 cathode material. All electrochemical properties tests were performed in an electrochemical workstation (CorrTest, CS310M). Inductively coupled plasma-optical emission spectrometry (ICP-OES, FHS12, Spectro Arcos) was utilized to measure the concentration of metal ions.

**Table S1** XRF and EDX analysis of EOL cathode material.

| **XRF** | **$Co_3O_4$** | **NiO** | **MnO** | **F** | **$Al_2O_3$** | |
|---|---|---|---|---|---|---|
| **wt%** | 76.63 | 10.54 | 7.91 | 3.88 | 1.04 | |
| **StdErr** | 0.17 | 0.07 | 0.10 | 0.39 | 0.07 | |
| **EDX** | **Co** | **Ni** | **Mn** | **F** | **Al** | **O** |
| **wt%** | 56.6 | 4.28 | 3.34 | 0.882 | 0.698 | 34.2 |

**Table S2** Leaching efficiency results of Li (a), Co (b), Ni (c), and Mn (d) with various acids ratios at 40 min and 10 g/L solid-liquid ratio.

| **Various acids ratios/M** | | | **Leaching efficiency results/%** | | | |
|---|---|---|---|---|---|---|
| **HCl** | **$HNO_3$** | **VC** | **Li** | **Co** | **Ni** | **Mn** |
| 0 | 0 | 1 | 98.00 | 96.69 | 99.57 | 99.90 |
| 0 | 1 | 0 | 61.35 | 10.40 | 58.84 | 15.36 |
| 0.25 | 0.25 | 0.5 | 99.50 | 95.60 | 98.10 | 98.80 |
| 0.25 | 0.5 | 0.25 | 99.78 | 98.10 | 99.23 | 99.83 |
| 0.5 | 0.25 | 0.25 | 99.82 | 99.89 | 99.40 | 99.92 |
| 1 | 0 | 0 | 93.43 | 66.73 | 95.97 | 80.70 |

The introduction of ascorbic acid for the recycling of waste cathode material has already been reported due to its acidity and reducibility. However, ascorbic acid is a very expensive reducing agent, the extensive use will undoubtedly increase operating costs. In this paper, the amount of VC required to treat 2 kg of spent lithium-ion batteries is calculated.

**Table S3** The amount of VC required to treat 2 kg of spent lithium-ion batteries

| Acid solution | Cathode active material/kg | VC/kg |
|---|---|---|
| **ascorbic acid** | 0.7 | 11.848 |
| **mixing acids** | 0.7 | 2.962 |

**Table S4** Leaching efficiencies and EDX analysis of the leached cathode material.

| ICP-OES | Co | Ni | Mn | Li | Al | | |
|---|---|---|---|---|---|---|---|
| **LR(%)** | 99.98 | 99.98 | 99.99 | 99.99 | 87.15 | | |
| **EDX** | Co | Ni | Mn | F | Al | C | O |
| **wt%** | -- | -- | -- | 5.24 | 52.63 | 5.65 | 36.48 |

**Table S5** XPS parameters obtained from the leached spent cathode materials.

| Line designation | Composition | FWHM (eV) | Area (cps•eV) | $E_b$ (eV) |
|---|---|---|---|---|
| **Al 2*p*** | $Al_2O_3$ [1] | 3.4 | 2154.6 | 71.1 |
| **Al 2$p_{3/2}$** | $Al_2O_3$ [2] | 1.6 | 12028.8 | 74.1 |
| **Co 2$p_{3/2}$** | $Co_3O_4$ [3] | 1.6 | 50528.4 | 779.3 |
| **Co 2$p_{3/2}$** | CoO [4] | 3.0 | 95148.5 | 780.3 |
| **Co 2$p_{1/2}$** | $Co_3O_4$ [5] | 1.4 | 16656.5 | 794.6 |
| **Co 2$p_{1/2}$** | $Co_3O_4$ [6] | 2.8 | 40665.5 | 795.9 |
| **O 1*s*** | $Co_3O_4$ [5] | 1.3 | 58883 | 529.35 |
| **O 1*s*** | CoO [7] | 2.0 | 49892 | 530.4 |
| **O 1*s*** | $Al_2O_3$ [8] | 2.9 | 91879 | 531.15 |

When $Al(OH)_3$, NCM622 precursor and $Li_2CO_3$ precipitate, there was a certain capacity loss of Li. Among them, the loss of precipitated $Al(OH)_3$ is about 1% -3%, the loss of precipitated NCM622 precursor is about 3% -5%, and the loss of precipitated $Li_2CO_3$ is about 6% -10%. And the recovered $Li_2CO_3$ can be utilized for the manufacturing of NCM 622 cathode material. The NCM622 precursor was mixed with $Li_2CO_3$ at a Li/M (M is the sum of transition metals Ni, Co, Mn) molar ratio of 1.06, so additional extra $Li_2CO_3$ is required.

**Table S6** Variation of metal concentration in recovery process.

| Solution | Concentration of element/M | | | |
|---|---|---|---|---|
| | Li | Co | Ni | Mn |
| **the effluent** | 0.101 | 0.074 | 0.006 | 0.021 |
| **concentration adjustment** | 0.99 | 0.072 | 0.215 | 0.071 |
| **NCM622 precipitation finished** | 0.95 | -- | -- | -- |
| **$Li_2CO_3$ precipitation finished** | 0.062 | -- | -- | -- |

**Table S7** [9,10] A comprehensive summary of the kinetic models.

| No. | Kinetic models | Name |
|---|---|---|
| **D1** | $kt = \alpha^2$ | One-dimensional diffusion model |
| **D2** | $kt = (1-\alpha)\ln(1-\alpha)+\alpha$ | Two-dimensional diffusion model |
| **D3** | $kt = [1-(1-\alpha)^{1/3}]^2$ | Three-dimensional diffusion model (Jander) |
| **D4** | $kt = [1-(2\alpha/3)]-(1-\alpha)^{2/3}$ | Ginstling-Brounshtein model |
| **D5** | $kt = [1/(1-\alpha)^{1/3}-1]^2$ | Zhuravlev, Lesokhin and Templeman model |
| **D6** | $kt = [(1+\alpha)^{1/3}-1]^2$ | Three-dimensional diffusion model (Anti-Jander) |
| **D7** | $k\ln t = [1-(1-\alpha)^{1/3}]^2$ | Kroger and Ziegler model |
| **D8** | $kt = [1-(1-\alpha)^{1/2}]^2$ | Cylindrical diffusion model (Jander) |
| **D9** | $kt = [1-(1+\alpha)^{1/2}]^2$ | Cylindrical diffusion model (Anti-Jander) |
| **D10** | $kt = [1/((1-\alpha)^{1/3})]-1$ | Dickinson and Heal model |
| **D11** | $kt = [1/((1-\alpha)^{1/3})]-1+1/3\ln(1-\alpha)$ | Dickinson and Heal model |
| **D12** | $kt = 1/5(1-\alpha)^{-5/3}-1/4(1-\alpha)^{-4/3}+1/20$ | Dickinson and Heal model |
| **A1** | $kt = [-\ln(1-\alpha)]^{1/4}$ | Avrami-Erofeev model |
| **A2** | $kt = [-\ln(1-\alpha)]^{1/2}$ | Avrami-Erofeev model |
| **A3** | $kt = [-\ln(1-\alpha)]^{1/3}$ | Avrami-Erofeev model |
| **A4** | $kt = [-\ln(1-\alpha)]^{4/3}$ | Avrami-Erofeev model |
| **A5** | $kt = [-\ln(1-\alpha)]^{2/3}$ | Avrami-Erofeev model |
| **A6** | $\ln k+n\ln t = \ln[-\ln(1-\alpha)]$ | Avrami-Erofeev model |
| **F0** | $kt = \alpha$ | Zero order |
| **F1** | $kt = -\ln(1-\alpha)$ | First order |
| **F2** | $kt = (1-\alpha)^{-1}$ | Second order |
| **R2** | $kt = 1-(1-\alpha)^{1/2}$ | Interface (contracting area) |
| **R3** | $kt = 1-(1-\alpha)^{1/3}$ | Interface (contracting volume) |
| **R4** | $kt = 1-(1-\alpha)^{2/3}$ | Interface |
| **P1 (n=2)** | $kt = \alpha^{1/2}$ | Power law（half） |
| **P1 (n=3)** | $kt = \alpha^{1/3}$ | Power law（third） |
| **P1 (n=4)** | $kt =\alpha^{1/4}$ | Power law（quarter） |
| **E1** | $kt = \ln\alpha$ | Exponential |
| **E2** | $kt = [-\ln(1-\alpha)]^2$ | Exponential |
| **B1** | $kt = \ln[\alpha/(1-\alpha)]$ | Prout-Tompkinsmodel |

**Table S8** Regression parameters of Li, Co, Ni, and Mn.

| *T* (°C) | Li | | Co | | Ni | | Mn | |
|---|---|---|---|---|---|---|---|---|
| | *k* | $R^2$ | *k* | $R^2$ | *k* | $R^2$ | *k* | $R^2$ |
| **30** | 1.146 | 0.997 | 0.2832 | 0.998 | 0.2098 | 0.976 | 0.3519 | 0.991 |
| **50** | 1.965 | 0.978 | 0.3021 | 0.999 | 0.2913 | 0.983 | 0.4911 | 0.947 |
| **70** | 2.554 | 0.956 | 0.3364 | 0.999 | 0.3589 | 0.954 | 0.7198 | 0.951 |
| **90** | 5.512 | 0.986 | 0.3491 | 0.999 | 0.6236 | 0.999 | 1.210 | 0.878 |
| ***-ln*k/*(1000/*T*)*** | 2.715 | 0.953 | 0.4049 | 0.975 | 1.893 | 0.946 | 2.231 | 0.976 |

**Table S9** Lattice structure parameters of the NCM622 cathode material.

| Parameter | a(Å) | c(Å) | c/a | $I_{003}/I_{104}$ | Ni in Li layer (%) | $R_p$ (%) | $R_{wp}$ (%) |
|---|---|---|---|---|---|---|---|
| **NCM622** | 2.8731 | 14.2128 | 4.9468 | 1.90 | 0.97 | 7.57 | 8.14 |

## Nitrogen cycle

$NH_3H_2O$ solution is used to adjust the pH of the effluent. After $Al(OH)_3$, NCM622 precursor and $Li_2CO_3$ precipitation, calcium oxide can be introduced to the effluent to release the $NH_3$ gas with the help of reaction heat. Finally, $NH_3$ gas was pumped in water to obtain $NH_3{\cdot}H_2O$, thereby achieving the recycling of N element.

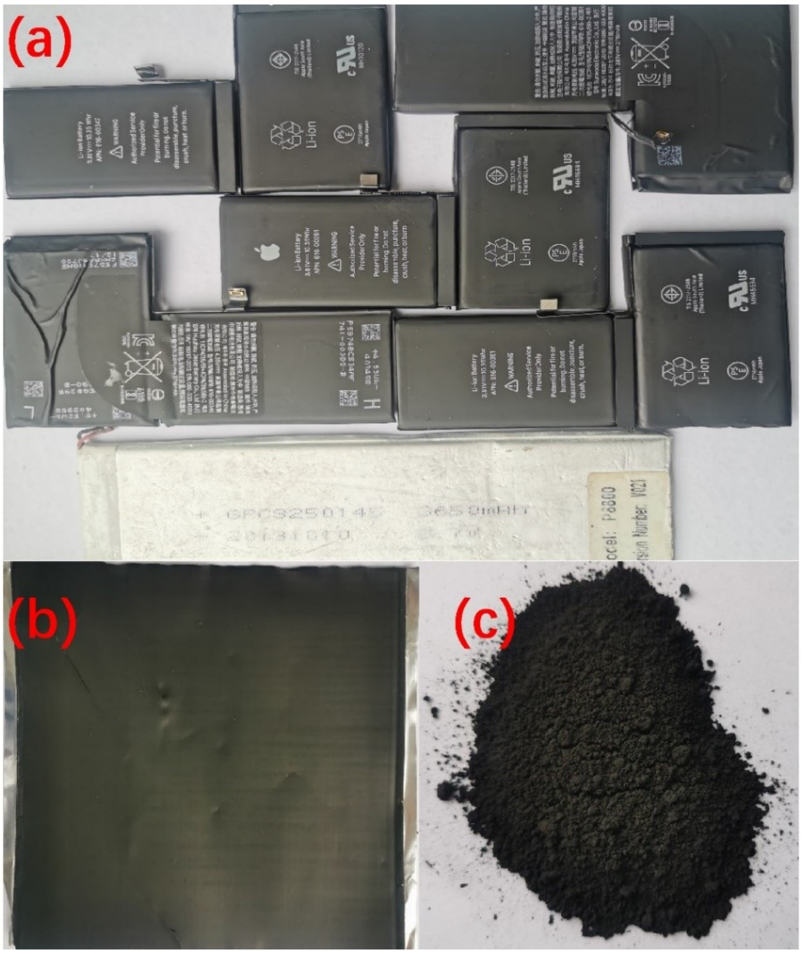


**Figure S1** EOL LIBs (a), cathode (b), and recovered cathode powders (c) from EOL LIBs.

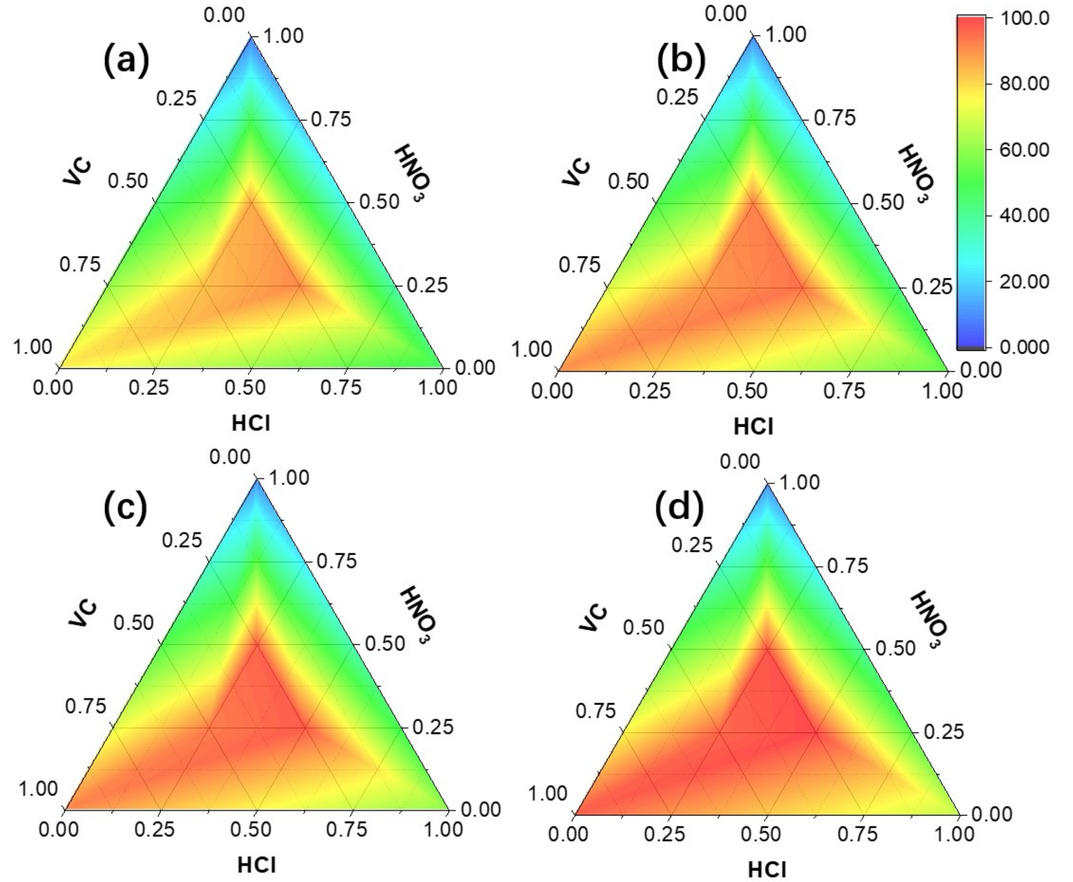


**Figure S2** Leaching kinetics of Co at 30 °C and 10 g/L solid-liquid ratio at 11min (a), 20 min (b), 30 min (c), and 40min (d) with various mixed acids ratios.

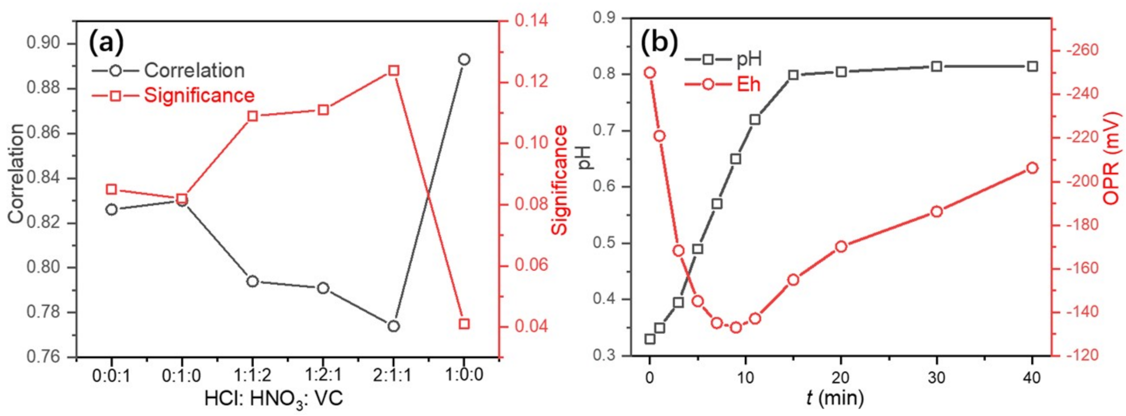


**Figure S3** Correlation and significance between mixed acids ratios and leaching efficiencies (a), Eh-pH diagram measured during the leaching process with 0.5 M HCl, 0.25 M $HNO_3$, and 0.25 M HCl at 30 °C and 10 g/L solid-liquid ratio (b).

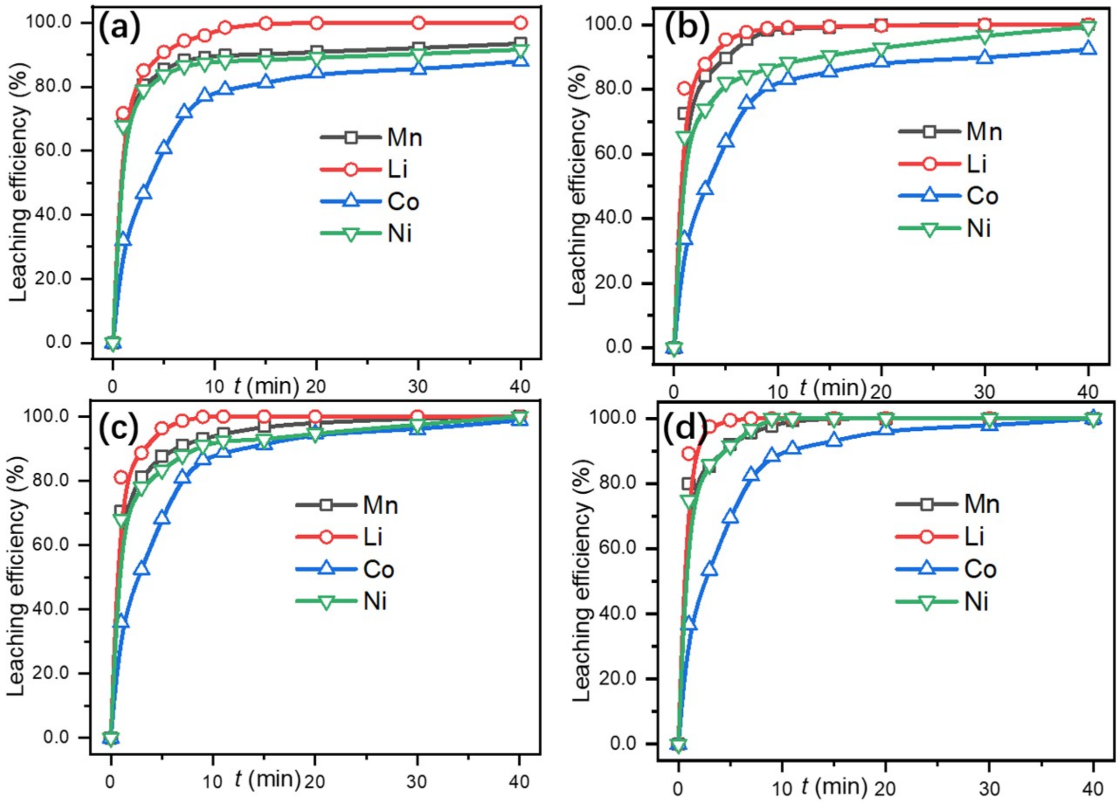


**Figure S4** Leaching kinetics of strategic metals at 30 °C (a), 50 °C (b), 70 °C (c), and 90 °C (d) at 10 g/L solid-liquid ratio, 0.5 M HCl, 0.25 M $HNO_3$ and 0.25 M VC.

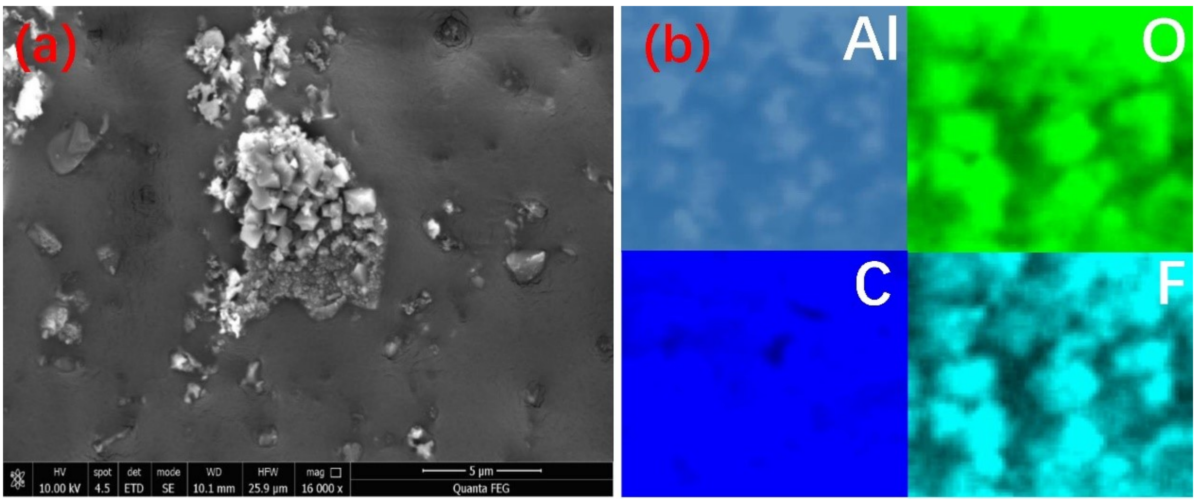


**Figure S5** SEM (a) and EDX (b) images of the leached residual at 90 °C with optimal acids ratios.

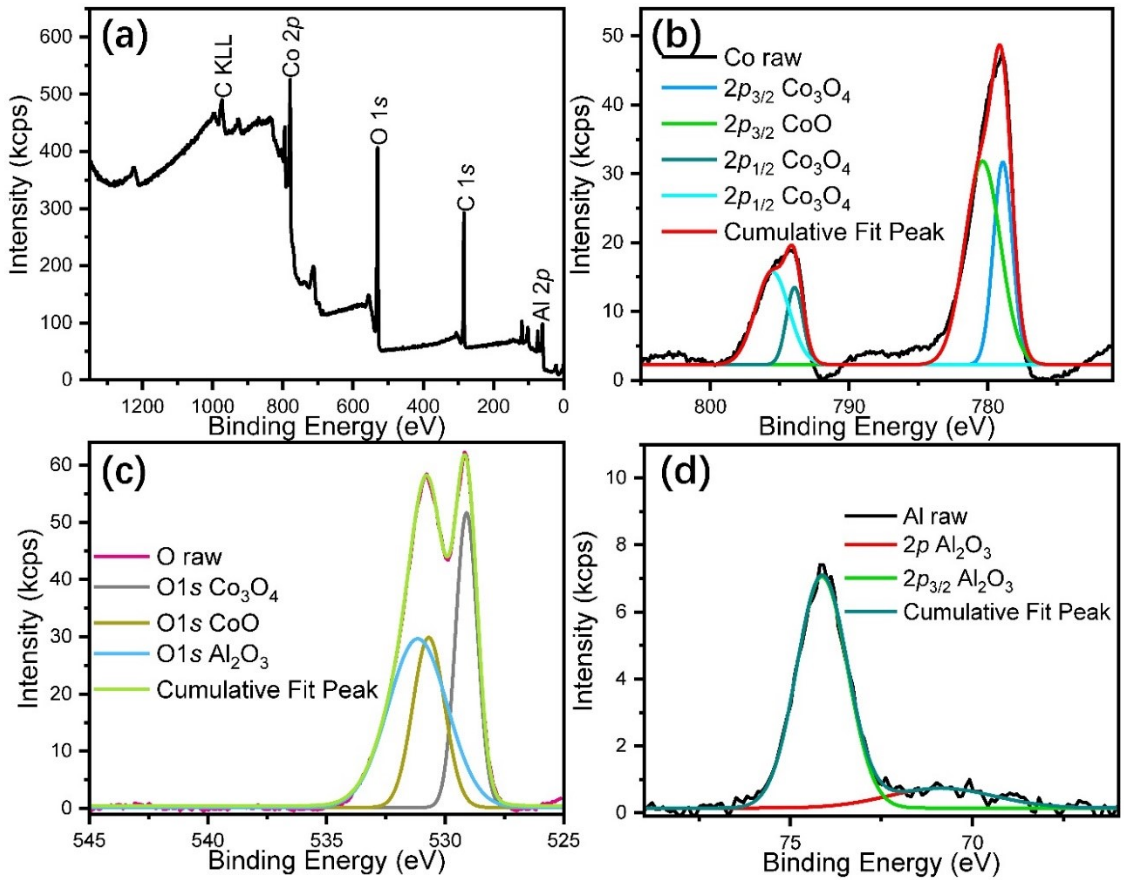


**Figure S6** XPS survey of the leached residual at 30 °C (a) and the deconvoluted high-resolution XPS curves of Co (b), O (c), and Al (d).

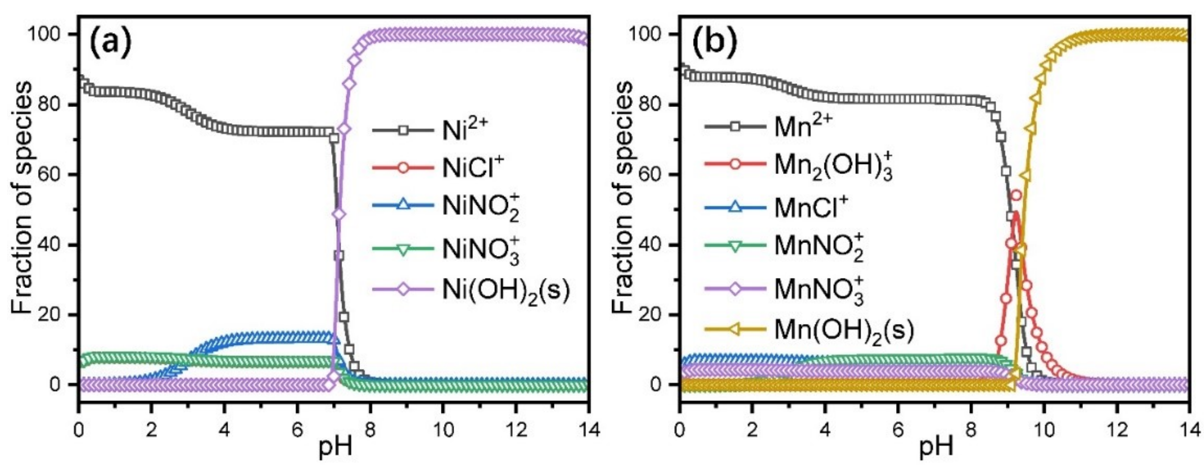


**Figure S7** Thermodynamic calculations of Ni-containing (a) and Mn-containing (b) species at 30°C.

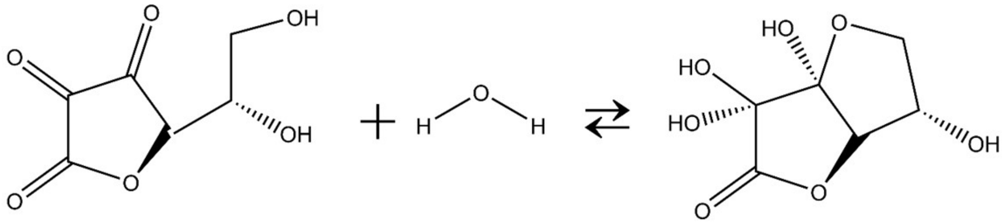

**Figure S8** Reactions of DHA hydrate to form Bi-DHA.

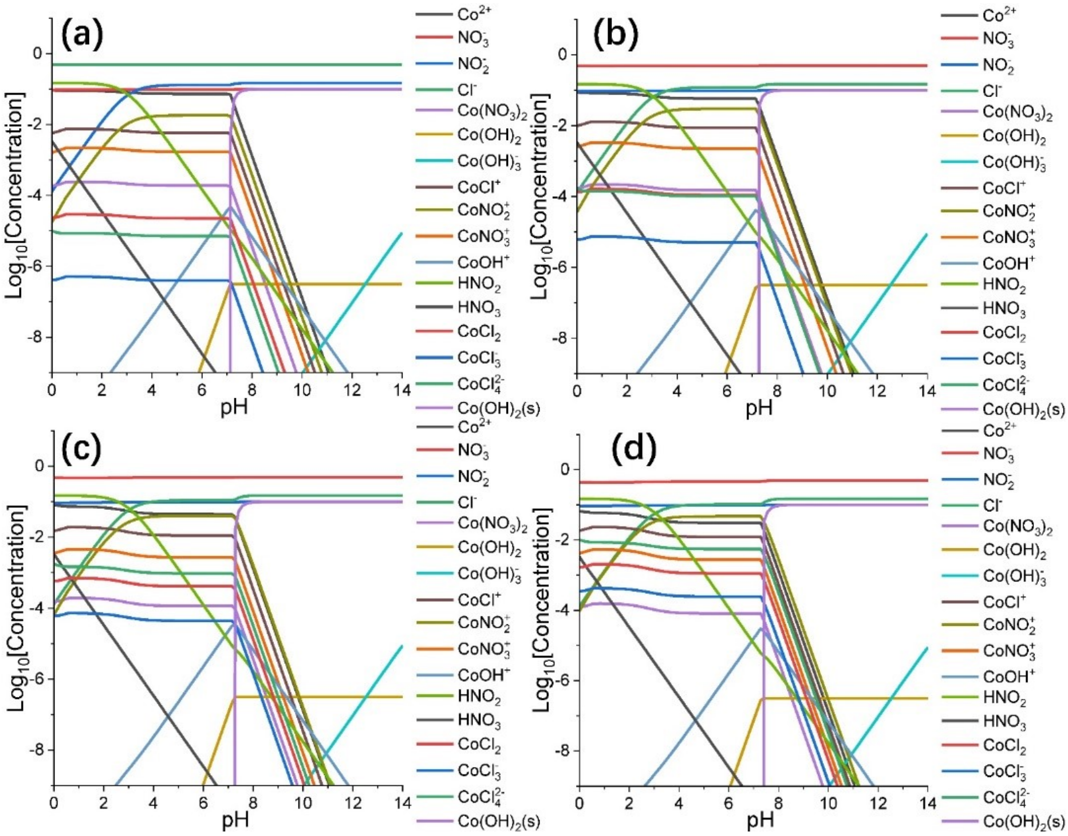


**Figure S9** Thermodynamic calculated species distributions of mixed acids system at 30 ℃ (a), 50 ℃ (b), 70 ℃ (c) and 90 ℃ (d).

S11

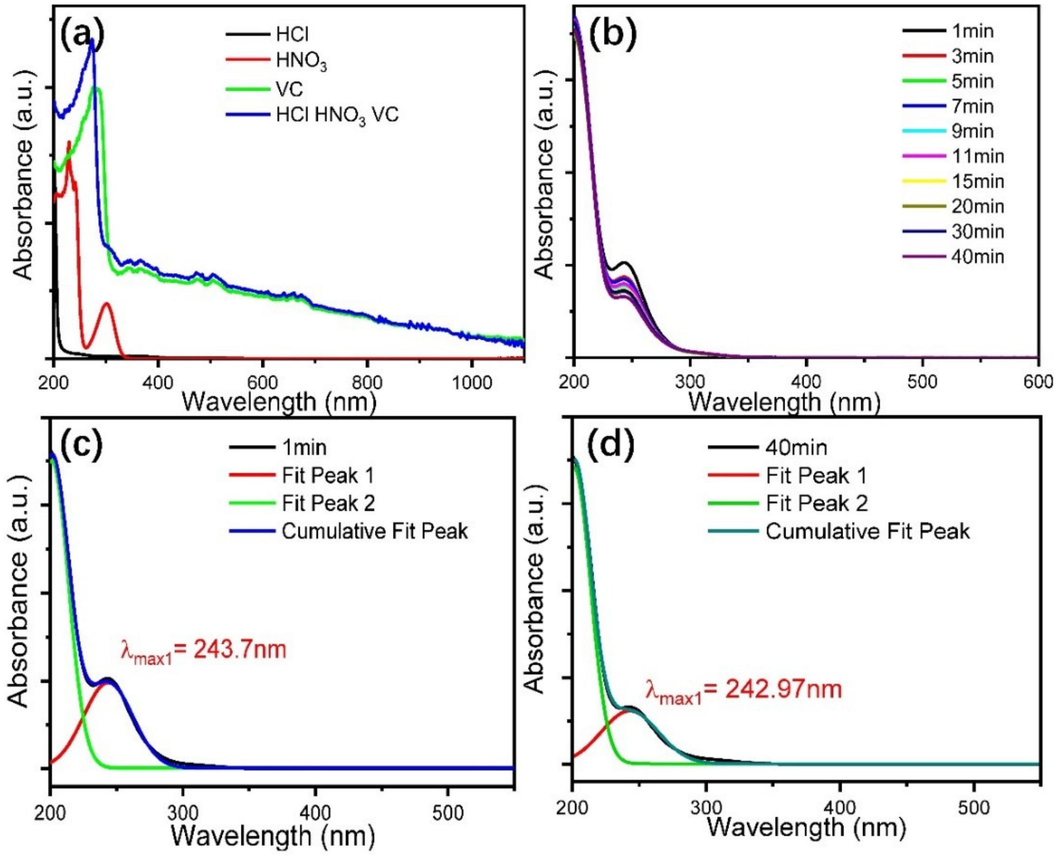


**Figure S10** UV-vis spectrum of mixed acids at 0min (a), 1~40 min (b), and deconvoluted absorbance curves at 1 min (c) and 40 min (d).

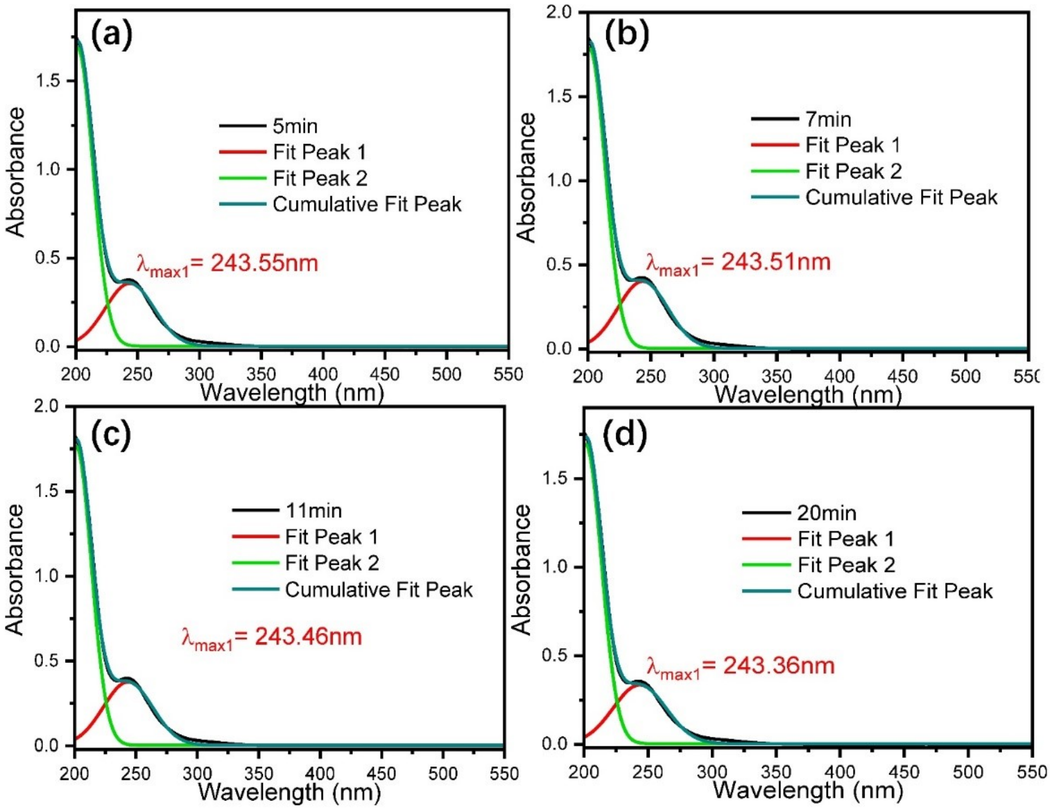


**Figure S11** Deconvoluted UV-vis absorbance in mixed acids system at 5 min (a), 7 min (b), 11 min (c), and 20 min (d).

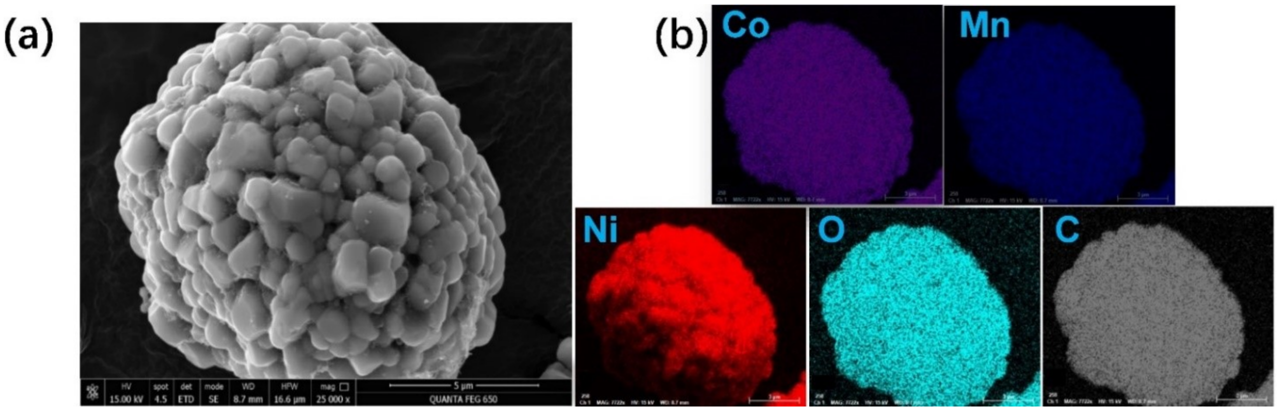


**Figure S12** SEM (c), and EDX (d) images of the as-recovered NCM622 precursor.

S13

**References**


[1] E. Gillet, B. Ealet, *Surf. Sci.*, 1992, **273**, 427-436.

[2] C. D. Wagner, D. E. Passoja, H. F. Hillery, et al., *Vac. Sci. Technol.*, 1982, **21**, 933-944.

[3] Haber, L. Ungier, J. Electron Spectrosc. *Relat. Phenom.*, 1977, **12**, 305-312.

[4] C. V. Schenck, J. G. Dillard, J. W. Murray, *J. Colloid Interface Sci.*, 1983, **95,** 398-409.

[5] G. Tyuliev, S. Angelov, *Appl. Surf. Sci.*, 1988, **32**, 381-391.

[6] B.J. Tan, K.J. Klabunde, P.M.A. Sherwood, *J. Am. Chem. Soc.*, 1991, **113,** 855-861.

[7] P. Porta, R. Dragone, G. Fierro, et al., *Chem. Soc. Faraday Trans., Faraday Transactions*, 1992, **88**, 311-319.

[8] V. I.Nefedov, *J. Electron Spectrosc. Relat. Phenom.*, 1982, **25**, 29-47.

[9] C.F. Dickinson, G.R. Heal, *Thermochimica Acta*, 1999, **340-341**, 89-103.

[10] J. H. Sharp, G. W. Brindley, B. N. N. Achar, *J. Am. Ceram. Soc.*, 1966, **49**, 379-382.